

# EPJ E

Soft Matter and  
Biological Physics

EPJ.org  
your physics journal

Eur. Phys. J. E (2011) **34**: 52

DOI: 10.1140/epje/i2011-11052-5

## **Analysis of the cluster formation in two-component cylindrical bottle-brush polymers under poor solvent conditions. A simulation study**

P.E. Theodorakis, W. Paul and K. Binder



Società  
Italiana  
di Fisica



Springer

# Analysis of the cluster formation in two-component cylindrical bottle-brush polymers under poor solvent conditions. A simulation study

P.E. Theodorakis<sup>1,2,3,4,a</sup>, W. Paul<sup>5</sup>, and K. Binder<sup>1</sup>

<sup>1</sup> Institut für Physik, Johannes Gutenberg-Universität D-55099 Mainz, Staudinger Weg 7, Germany

<sup>2</sup> Faculty of Physics, University of Vienna A-1090, Boltzmanngasse 5, Vienna, Austria

<sup>3</sup> Institute for Theoretical Physics and Center for Computational Materials Science (CMS), Technical University of Vienna A-1040 Vienna, Hauptstraße 8-10, Austria

<sup>4</sup> Vienna Computational Materials' Laboratory A-1090 Vienna, Sensengasse 8/12, Austria

<sup>5</sup> Institut für Physik, Martin-Luther-Universität Halle-Wittenberg, von Seckendorff-Platz 1, 06120 Halle, Germany

Received 22 February 2011

Published online: 25 May 2011 – © EDP Sciences / Società Italiana di Fisica / Springer-Verlag 2011

**Abstract.** Two-component bottle-brush polymers, where flexible side chains containing  $N = 20, 35$  and 50 effective monomers are grafted alternately to a rigid backbone, are studied by Molecular Dynamics simulations, varying the grafting density  $\sigma$  and the solvent quality. Whereas for poor solvents and large enough  $\sigma$  the molecular brush is a cylindrical object with monomers of different type occupying locally the two different halves of the cylinder, for intermediate values of  $\sigma$  an axially inhomogeneous structure of “pearl-necklace” type is formed, where microphase separation between monomers of different type within a cluster takes place. These “pearls” have a strongly non-spherical ellipsoidal shape, due to the fact that several side chains cluster together in one “pearl”. We discuss the resulting structures in detail and we present a comparison with the single-component bottle-brush case.

## 1 Introduction

The progress in chemical synthesis allows for the design of macromolecules of complex architectures, where the resulting structure of the synthesised molecules is controlled with remarkable accuracy [1,2]. Comb-like architectures have recently found particular interest, *i.e.*, bottle-brush polymers, where flexible linear or branched side chains are grafted regularly or randomly onto a backbone chain [1–13]. The interplay between steric repulsions of the side chain monomers and the effective attraction between monomers that can be tuned by the quality of the solvent results in intricate spatial self-organisation of these macromolecules. Built on this, many interesting applications have been envisaged [7–9] as external parameters may vary, *i.e.*, an applied electric field, irradiation by light, or simply changes in pH value of the solution, temperature, etc. Apart from these synthetic bottle-brush polymers, also biopolymers with a related architecture are abundant in nature. For instance, brush-like macromolecules that contain a protein backbone with carbo-

hydrate side chains known as proteoglycans [14], are held responsible for a large variety of very interesting biological functions (cell signalling, cell surface protection, joint lubrication, etc. [15–17]). Understanding the structure property relation of such bottle-brush macromolecules remains a challenging problem of statistical thermodynamics due to the multitude of the involved length scales resulting from their complex structure [18–55].

In the present work, we study the case of bottle-brush polymers with two different types of regularly grafted linear flexible chains (A, B) of the same length ( $N_A = N_B = N$ ) under poor solvent conditions. The backbone is considered rigid and periodic boundary conditions are applied at its ends as was done in previous studies [51,55–57], disregarding in this way any end effects (very long backbone chains) or effects due to the flexibility of the backbone. In fact, the backbone gets stiffened as a natural effect of the steric repulsions between monomers with an increase of the grafting density or of the length of the side chains, in addition to its intrinsic stiffness due to the interactions of the constituent monomers [2,48,10,11,53,54]. Moreover, it has been shown for large grafting density and good solvent conditions that the local structure in a bottle-brush

<sup>a</sup> e-mail: panagiotis.theodorakis@univie.ac.at

polymer with flexible backbone is almost indistinguishable from that with a rigid backbone [52]. It was shown that flexible side chains collapse individually on the rigid backbone upon decrease of the temperature when the grafting density is low enough that neighbouring side chains do not come into contact [51, 55, 56]. Increase of the grafting density gives rise to “pearl-necklace” structures [43, 51, 56], where clusters containing more than one side chain are formed and microphase separation of dumbbell-type between A and B monomers within a “pearl” is observed [55]. Further increase of the grafting density results in structures in the form of “Janus cylinders” or “Janus dumbbells” [8, 39, 41, 46, 47, 55], *i.e.*, the cylinder splits in two halves, such that the A-B interface contains the cylinder axis (taken to be along the  $z$ -axis henceforth). In an effort to understand the transitions between the different states we analyse quantities related to the formed clusters as a whole (A and B monomers within a cluster), as well as separately considering only A-type or B-type monomers within a cluster, exploring the statistical mechanics of a coarse-grained model by computer simulation methods. Our data will be also discussed in the context of recent molecular dynamics results for the case of single-component bottle-brush polymers, which were already compared with scaling predictions, reported elsewhere [43, 56].

Of course, the present model is not expected to describe real bottle-brush molecules with fully flexible backbone chains in poor solvents at the considered intermediate grafting density, since such a system is expected to collapse further into a globular, rather dense structure, which has then a much larger number of favorable “contacts” between monomers than the pearl-necklace type structures considered in the present paper. In fact, early simulations on a related model confirmed this prediction [58]. We plan to extend our studies to this flexible backbone limit also for our model, and then the present work will be a very useful “benchmark” case to compare to, and clarify precisely the conditions for which backbone flexibility makes a significant difference. In addition, we want to mention that particularly in a biological context many macromolecules occur which intrinsically are very stiff. For side chains grafted to such rigid chains, the so-called “hairy rods” [2], our model would be qualitatively realistic; certain neurofilaments [59–62] are an example for this case. It is also conceivable to graft chains to carbon nanotubes (which may be useful to avoid bundle formation of nanotubes, similarly as grafting chains to colloids [63] or nanoparticles [64] is useful to avoid aggregation of such particles). Finally, we mention that interesting pearl-necklace structures have in fact been observed for core-shell bottle-brushes [65].

The remainder of this paper is organized as follows. In sect. 2, we describe our model and sketch the analysis needed to characterise size and shape (and other properties) of the “pearls” quantitatively, considering not only average properties, but also fluctuations. Section 3 presents our numerical results, while sect. 4 summarises our conclusions.

## 2 Model and methods to analyse the results

In this study we consider the most symmetric case of bottle-brush polymers with two types of side chains A, B, where the length of the side chains A equals that of B chains ( $N_A = N_B = N$ ). We consider only rather short side chain lengths, namely  $N = 20, 35$  and  $50$ . It is clear that the interpretation of the results for such rather short chains in terms of scaling concepts would be a delicate matter, however, we emphasise that our range of  $N$  corresponds nicely to the range of  $N$  available in experiments on bottle-brushes [1, 2, 10, 11, 53]. Still, as an interesting theoretical albeit academic problem it would be nice to extend our study to side chain lengths of several hundreds of effective monomers, but this is prohibitively difficult in the poor solvent regime, where relaxation times of the chains get very long. The side chains are grafted regularly and alternately onto the rigid backbone with grafting density  $\sigma$ , *i.e.*, the distance between two neighbouring grafting sites is  $1/\sigma$ . The total number of grafted A and B chains is typically  $M = 50$ . As discussed above, we consider the backbone as an immobile straight line in the  $z$ -direction, where we also apply periodic boundary conditions, thus disregarding any end-effects. In  $(x, y)$ -directions periodic boundary conditions were chosen as well, but the considered linear dimensions of the simulation box were large enough, so that never any interaction of the bottle-brush polymer with its periodic images could occur in these directions.

The side chains are modelled by the standard bead-spring model that has been extensively used in the literature for related work [24, 66–71] (*e.g.*, polymer brushes grafted to flat walls [67–71] or cylinders [24], with most of this work being restricted to good solvent conditions). All beads interact with a truncated and shifted Lennard-Jones (LJ) potential

$$U_{\text{LJ}}(r) = \begin{cases} 4\epsilon_{\text{LJ}}[(\sigma_{\text{LJ}}/r)^{12} - (\sigma_{\text{LJ}}/r)^6] + C, & r \leq r_c, \\ 0, & r > r_c, \end{cases} \quad (1)$$

where  $r_c = 2.5\sigma_{\text{LJ}}$  is the cut-off of the potential, and the constant  $C$  is defined such that  $U_{\text{LJ}}(r = r_c)$  is continuous at this cut-off. Henceforth, units are chosen such that  $\epsilon_{\text{LJ}} = 1$ ,  $\sigma_{\text{LJ}} = 1$ ,  $k_B = 1$ , and  $m = 1$  (mass of the beads) for simplicity. When we consider two types (A, B) of side chains, we still use  $\sigma_{\text{LJ}}^{\text{AA}} = \sigma_{\text{LJ}}^{\text{AB}} = \sigma_{\text{LJ}}^{\text{BB}} = 1$  and  $\epsilon_{\text{LJ}}^{\text{AA}} = \epsilon_{\text{LJ}}^{\text{BB}} = 1$ , but  $\epsilon_{\text{LJ}}^{\text{AB}} = 1/2$  to create an un-mixing tendency. We know that in the case of a binary system with monomers at density  $\rho = 1$  (*e.g.*, a LJ mixture which is a standard system for the study of phase separation), macroscopic phase separation occurs below a critical temperature  $T_c \approx 1.5$  [72]. For our bottle-brush polymers the average densities are much smaller, especially at distances far from the backbone, but since the critical temperature scales proportional to the chain length, we are able to detect microphase separation with our model [55, 57].

The connectivity of the beads along the chain is maintained by the finitely extensible nonlinear elastic (FENE)

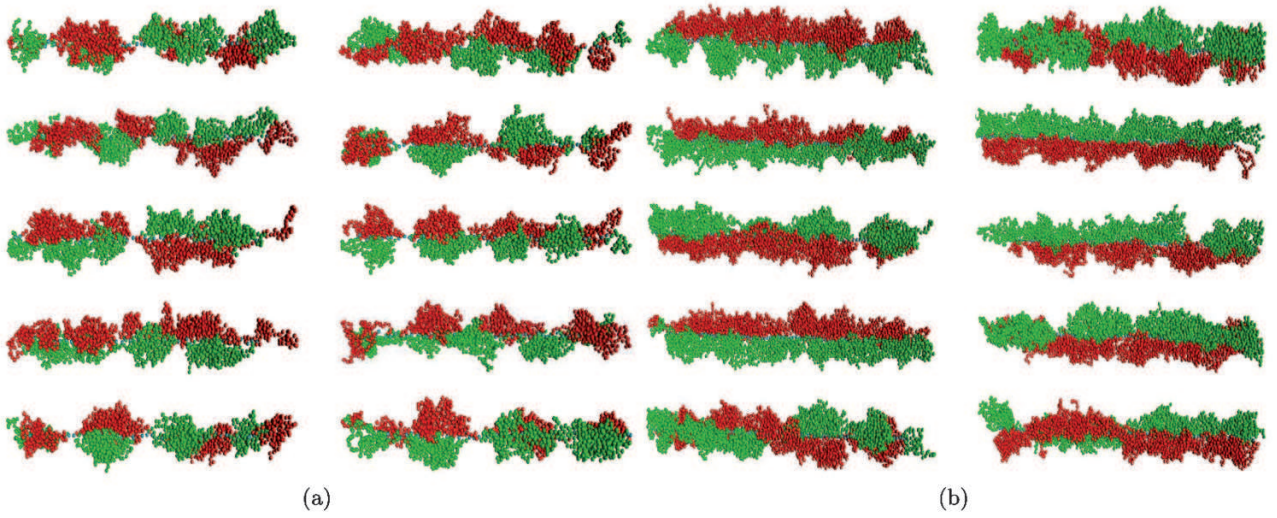


**Fig. 1.** (Colour online) Snapshot pictures of bottle-brush polymers at  $\sigma = 0.76$ ,  $N = 35$ ,  $T = 1.5$  (50 grafted chains) (a), and  $\sigma = 1.14$ ,  $N = 35$ ,  $T = 1.5$  (100 grafted chains) (b). A and B monomers are distinguished by different colour (or light grey *vs.* dark grey, respectively).

potential

$$U_{\text{FENE}}(r) = -\frac{1}{2}kr_0^2 \ln[1 - (r/r_0)^2], \quad 0 < r \leq r_0, \quad (2)$$

where the standard choice of parameters ( $r_0 = 1.5$  and  $k = 30$ ) was adopted, and  $U_{\text{FENE}}(r > r_0) = \infty$ .

For the model defined by eq. (1) and (2) the Theta temperature is known,  $\Theta \approx 3.0$  [70]. Being interested in  $T \leq \Theta$ , we have studied the temperature range  $1.5 \leq T \leq 3.0$ . Note that no explicit solvent particles are included; solvent quality is taken into account in the simulations only implicitly, as is standard practice [67], by varying the temperature of the system. The temperature is controlled by the Langevin thermostat, as done in previous work [51,55–57]. The equations of motion for the coordinates  $\{\mathbf{r}_i(t)\}$  of the beads

$$m \frac{d^2 \mathbf{r}_i}{dt^2} = -\nabla U_i - m\gamma \frac{d\mathbf{r}_i}{dt} + \mathbf{F}_i(t) \quad (3)$$

are numerically integrated using the GROMACS package [73]. In eq. (3),  $t$  denotes time,  $U_i$  is the total potential the  $i$ -th bead experiences,  $\gamma$  is the friction coefficient, and  $\mathbf{F}_i(t)$  the random force.  $\gamma$  and  $\mathbf{F}_i(t)$  are related by the fluctuation-dissipation relation

$$\langle \mathbf{F}_i(t) \cdot \mathbf{F}_j(t') \rangle = 6k_B T \gamma \delta_{ij} \delta(t - t'). \quad (4)$$

As in previous work, [51,55–57,66–68] the friction coefficient was chosen as  $\gamma = 0.5$ . For the integration of eq. (3) the leap frog algorithm [74] was used with a time step of  $\Delta t = 0.006\tau$ , where the natural time unit is defined as  $\tau = (m\sigma_{\text{LJ}}^2/\epsilon_{\text{LJ}})^{1/2} = 1$ .

We emphasise that equilibration of collapsed chains via MD methods is difficult, and thus we briefly describe here our equilibration procedure. First the system was equilibrated at  $T = 3.0$  for a time range of  $30 \times 10^6\tau$ . To gather

statistics, a sufficient number of statistically independent configurations (typically 500) at this temperature was used as initial configurations of slow cooling runs, where the temperature  $T$  was lowered in steps of  $\Delta T = 0.1$ , running the system at each  $T$  for  $2 \times 10^6\tau$ . The final configuration of each (higher)  $T$  was used as starting configuration for the next (lower)  $T$ . In this way, we are able to generate statistically independent configurations of very dense systems throughout the studied temperature range. Note that in quasi-one-dimensional systems with short-range forces, a spontaneous symmetry breaking in the sense of well-defined sharp phase transitions cannot occur [75]. However, as the length of the chains increases, equilibration becomes exceedingly difficult, which prevented us from studying longer chains. Full thermal equilibrium would require that a chain which is part of a cluster disengages from this cluster and becomes part of a neighboring cluster, and only if many such transitions occur, structures as shown in fig. 1a are fully equilibrated. The time scale for such processes is expected to increase exponentially with the side chain length. We tried to avoid this problem by slow cooling from high  $T$  for an ensemble of statistically independent configurations, as stated above.

Based on previous experience with this system [55,57] the chosen ranges of side chain length, temperature and grafting density can be expected to reveal the most interesting structural transitions occurring in our model. One can see already from the snapshot pictures of fig. 1 the different morphologies that occur at temperature  $T = 1.5$  for bottle-brush polymers of different grafting density. At low grafting density, the side chains collapse onto the backbone forming globular objects, and this is not at all different from what is happening when we consider a single-component bottle-brush. Every cluster that is formed contains only one side chain. As the grafting density increases to intermediate values, rather dense clusters along the backbone containing several side chains occur (fig. 1a).

Within a cluster, microphase separation between A and B monomers is taking place and we expect in this case a different behaviour with respect to the single-component case. At high grafting densities (*e.g.*,  $\sigma = 1.14$  (fig. 1b)) conformations in the form of Janus-cylinder-type appear, where the A and B monomers occupy locally the two different halves of the cylinder. The interface between A and B monomers is along the backbone axes, whereas in the case of single-component bottle-brushes a homogeneous cylinder is formed.

When the chains collapse at low temperatures to form microphase-separated cluster structures, there is no reason *a priori* for the system to decide which side chains will belong to a specific cluster of the same type of monomers, due to the symmetry of our model. We actually observe fluctuations where a side chain of type A or B that was part of a cluster of similar monomers escapes from the cluster to become part of another neighbouring cluster with chains of the same type of monomers. In fact, these fluctuations are the slowest relaxation process in the system leading to complete thermodynamic equilibrium. As discussed above, the necessity to study cooling runs stems from the impossibility to perform simulations which are long compared to this time scale so that many of these exchanges of chains between clusters can be observed.

In the analysis, we distinguish between A, respectively, B clusters to study the microphase separation in our model system and clusters defined by neighbouring monomers, irrespective of whether they are of A or B type, to monitor the phase separation from the poor solvent at low temperatures. We remind the reader that we chose the solvent quality to be the same for A and B monomers. To identify the clusters, we have used the Stillinger [76] neighbourhood criterion for monomers: if two monomers are less than a distance  $r_n$  apart, they belong to the same cluster. We followed the standard choice  $r_n = 1.5\sigma_{LJ}$  and checked that qualitatively very similar results were obtained if one chooses  $r_n$  slightly smaller than this choice (larger values of  $r_n$  are physically hardly significant, since then the particles are too weakly bound, due to the rapid fall-off of the LJ potential). Due to the symmetrically chosen set of parameters for A and B monomers, the statistical analysis for A and B clusters should end up in the same results. This is confirmed by our results, validating our choice of simulation procedure.

Properties,  $F$ , depending on the fluctuating number of clusters, should be averaged with the probability  $P(x)$  that a number of clusters per side chain occurs, *i.e.*,

$$\bar{F} = \sum_x P(x)F(x). \quad (5)$$

In fig. 2 we are showing this distribution in the number of clusters per chain  $P(x)$  for several choices of side chain length  $N$  and for clusters of A and B monomers (fig. 2a-c) and for clusters of only A or B monomers (fig. 2d-f). For comparison, in the cases of (a)-(c) the corresponding data for the one-component bottle-brush polymer are also plotted. The first extreme case would be that each grafted side chain forms a separate cluster ( $x = 1$ ) with probability  $P(x) = 1$ . In this case a side chain never forms a

“contact” with a neighbouring chain, and the formation of clusters containing many side chains does not take place. This is shown in case (d), (e) and (f) for  $\sigma = 0.08$  to happen for all chain lengths  $N = 20, 35$  and  $50$ . The second extreme case would be that all chains are always forming one cluster ( $x = 1/M$ ) with probability  $P(x) = 1$ , which is not seen for any of our cases. In case (c) this occurs for  $\sigma = 0.76$  with a probability  $P(x) \approx 0.9$ . Of course, this case does occur for significantly higher grafting densities, such as  $\sigma = 1.14$ , see fig. 1b, but this is out of our interest here, where we focus on the pearl-necklace structures. Due to the incompatibility between A and B monomers there is always the small probability for a cluster to be split into several clusters, and this makes already a significant physical difference with the case of single-component bottle-brushes. Thus, comparing the data for the two-component bottle-brushes (fig. 2a-c, full symbols) and the single-component brush (fig. 2a-c, open symbols), we can clearly see at intermediate grafting densities that the peaks for the single-component bottle-brushes are shifted to the left. This is a clear indication that in the single-component bottle-brushes more side chains are able to come together and form clusters, compared with a corresponding (same  $\sigma$  and  $N$ ) two-component bottle-brush at low to intermediate grafting densities. At intermediate to higher grafting densities (*i.e.*,  $\sigma = 0.57$  and  $0.76$ ), the opposite effect is seen. At these grafting densities, the side chains are close enough that the incompatibility between A and B monomers increases the axial dimensions of the chains (see fig. 5), increasing in this way the probability of cluster formation. As the chain length increases, the incompatibility between A and B chains also increases, and the formation of clusters of A and B monomers becomes more probable. We also note that the analysis of the clusters becomes insignificant as the grafting density becomes very high since we impose in this case the neighbouring grafted chains to be at a distance smaller than 1.5, which is our criterion for defining a “contact”. However, as A- and B-type chains repel each other, we studied grafting densities up to  $\sigma = 0.76$  and thus distances between grafting sites  $1/\sigma = 1/0.76$ . Moreover, strong finite-size effects are expected in the case that a single cluster is formed with a high probability, due to the finite size of the backbone, as periodic boundary conditions are applied at both backbone ends. As we have grafted the A and B chains alternatingly, the minimum distance between a chain A and a neighbouring A chain is  $2/\sigma$ , while  $1/\sigma$  is the distance between neighbouring A and B chains. For this reason all the curves in cases (d), (e), and (f) of fig. 2 are shifted correspondingly to the right compared to the cases (a), (b), and (c). Increasing the chain length  $N$  shifts the curves to the left, showing that the formation of the clusters is more probable. However, one should keep in mind that increase of  $N$  eventually leads to the increase of incompatibility between A and B chains. All these phenomena endow the bottle-brushes with two types of grafted side chains with interesting additional properties compared with the case of a single-component bottle-brush.

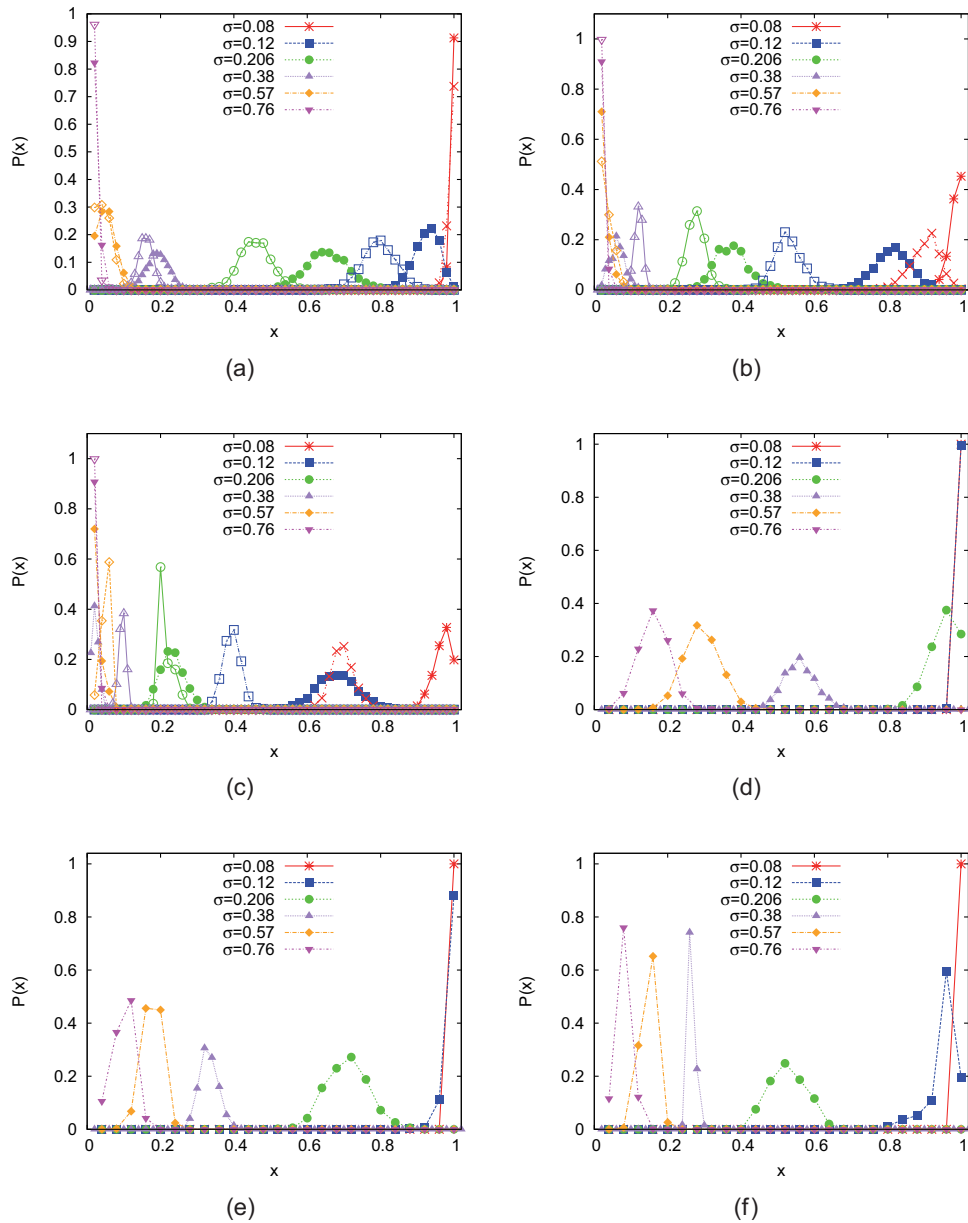


**Fig. 2.** (Colour online) Probability distribution  $P(x)$  of the number of clusters per chain plotted *vs.*  $x = N_{cl}/M$  for  $T = 1.5$ , and three choices of  $N$ :  $N = 20$  (a), 35 (b), and 50 (c). Grafting densities shown are  $\sigma = 0.08, 0.12, 0.206, 0.38, 0.57$ , and  $0.76$ . In cases (a), (b), and (c) the clusters are considered consisting of A and B beads both (full symbols and stars). Open symbols (and symbol  $\times$ ) correspond to results for the single-component bottle-brushes. The cases (d), (e), and (f) correspond to (a), (b), and (c), but A and B monomers are considered to form separate clusters.

### 3 Results and discussion

In fig. 3 we are presenting the average number of clusters per chain  $\bar{x}$  plotted *versus*  $\sigma$ . Figure 3(a) represents the case where we consider clusters containing both A and B monomers. One can clearly recognise the trivial regime  $\bar{x} = 1$ , where each cluster contains only one chain of A or B monomers. As the grafting density increases, this ratio takes values lower than 1 denoting the onset of the pearl-necklace regime. This transition becomes sharper as the length of the side chains increases and the curves for these intermediate grafting densities are shifted to the left. For

a fixed side chain length at higher temperature ( $T = 2.0$ ) the formation of a higher number of clusters along the backbone becomes more favourable. The transition from the pearl-necklace regime to the case that all chains form a single cluster (Janus type) occurs gradually for grafting densities higher than  $\sigma \approx 0.5$ . If we compare this result with that of the single-component bottle-brushes (fig. 3c), we see that the onset of pearl-necklace structures occurs at a smaller grafting density and also the number of formed clusters is smaller, showing that, due to the incompatibility between A and B monomers, the clusters of A and B monomers obtain a more elongated structure, *i.e.*, they

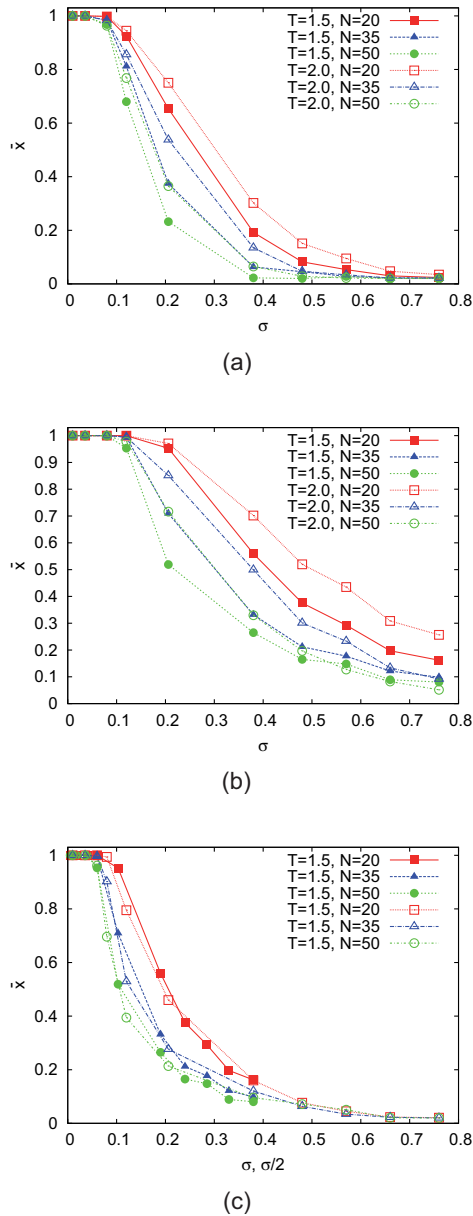


**Fig. 3.** (Colour online) Average number of clusters per grafted chain  $\bar{x}$  plotted *vs.* grafting density  $\sigma$  at  $T = 1.5$  (full symbols) and  $T = 2.0$  (open symbols) for three different chain lengths as indicated, for A and B monomers in a cluster (a) and for A or B monomers ( $M$  corresponds to the number of A or B chains here) in a cluster (b). In part (c) we are plotting the results from (b) for  $T = 1.5$  *versus*  $\sigma/2$  (full symbols) and compare them with the data for the single-component bottle-brushes plotted *versus*  $\sigma$  (open symbols).

try to rearrange in such a way along the backbone that A and B contacts become fewer. If we consider only clusters of A or B monomers, then the transition from the trivial regime to the pearl-necklace regime is considerably shifted to the right, *i.e.*, to higher values of  $\sigma$ . This shift is about a factor of 2. Indeed, the distance between neighbouring A or B chains is  $2/\sigma$ , whereas between A and B neighbouring chains is  $1/\sigma$ , so this shift is expected. The

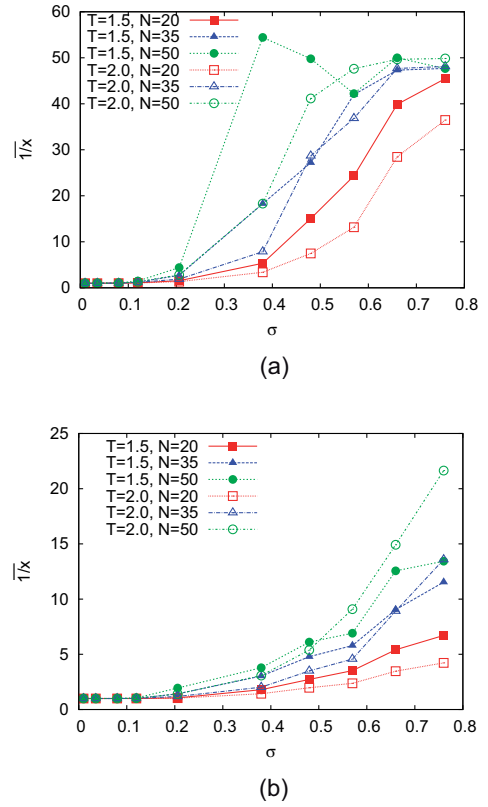


**Fig. 4.** (Colour online) Similar as in fig. 3, but on the ordinate axis the average number of chains in a cluster, *i.e.*,  $1/\bar{x}$ , is shown.

slope of the curves in the pearl-necklace regime becomes considerably smaller, showing that all transitions from the trivial to the pearl-necklace regime and from this to the homogeneous regime (Janus-type cylinders) are becoming smoother. Taking the trivial reduction of grafting density for either A or B clusters into account, by plotting the data from fig. 3b *versus*  $\sigma/2$  and comparing them with the results for the homopolymer brushes plotted *versus*  $\sigma$  as we have done in fig. 3c, reveals that within the accuracy of our data, both data sets agree. For grafting density  $\sigma \approx 0.8$  the transition to the Janus-cylinder-type regime has not been completed for most of the presented cases, except for the case  $N = 50, \sigma = 0.76$ . We also note here that for high grafting densities strong finite-size effects are expected due to the finite size of the backbone and the applied periodic boundary conditions. These effects are stronger in the case of longer side chains at a specific grafting density.

The different regions of the crossover from isolated chains to a single cluster at high grafting density are highlighted differently when we plot  $1/\bar{x}$  as a function of  $\sigma$  (fig. 4) instead of  $\bar{x}$  as in fig. 3. Whereas for a single-component bottle-brush the transition to the homogeneous chain is completed for all the presented chain lengths at grafting density  $\sigma \approx 0.80$  [56], in the case of two-component bottle-brushes a substantially protracted crossover is seen. This is clearly due to the strong concen-

tration fluctuations between A and B monomers, which result in the distortion of a single cluster formation even at this high grafting density. Only for the longest chains the cluster does not have any space to split in the  $z$ -direction and all chains belong to one cluster for the highest grafting densities. In fig. 4b, where we consider clusters only of monomers of one type (A or B), we are basically observing the same behaviour in the regime zero- $\sigma$  as on the left side in the regime zero- $\sigma/2$ . Considering the temperature variation, for  $N = 20$  we always find more chains per cluster at the lower temperature, whereas for  $N = 35$  and  $N = 50$  we are observing strong fluctuations, both in the case where clusters formed from both types of monomers are considered and for the case where pure A or B clusters are analysed. For the pure A or B clusters it seems that for the longest chains the number of chains per cluster is systematically smaller at the lower temperature, which corresponds nicely with the reduced parallel extension of the clusters shown in fig. 6.

Next we discuss the linear dimensions of the pearls and their dependence on the grafting density  $\sigma$ , readily obtained by computing the mean square gyration radius components  $\langle R_{g,z}^2 \rangle$  of the clusters in axial direction, as well as in radial direction  $\langle R_{g,xy}^2 \rangle$  (angular brackets denote thermal averaging). Figure 5 shows plots of  $\langle R_{g,xy}^2 \rangle$  versus  $\sigma$ . The horizontal part at low grafting densities shows the region where the clusters just contain individual collapsed chains, and there clearly cannot be a dependence on  $\sigma$ , of course. Then the pearl-necklace structure appears, and the size of the clusters in  $x$ - $y$  directions increases almost linearly, with the slope being higher when the length of the side chains  $N$  is higher. Of course, when the temperature is higher, also the size of the chains is larger, but the slopes corresponding to the pearl-necklace structures for different temperatures are similar, underlining the importance of the grafting density in the behaviour of our system.

At some point ( $\sigma \approx 0.5$ ), the size of the clusters in radial direction reaches a plateau regime the value of which depends on temperature. In the case where we consider clusters of only A or B chains, the size increases with a smaller slope and also the clusters are smaller in radial direction since in the other half of the plane a cluster of B chains occupies a part even in a pearl-necklace structure, as can naively visually be seen from the snapshots of fig. 1. Therefore, the result depicted in fig. 5b looks like a magnified picture of what is happening at low grafting densities in fig. 5a. If we compare with the results of the single-component bottle-brush shown in fig. 5c, we can say that the latter is the intermediate case between (a) and (b). The plateau at high grafting densities is not very pronounced and appears for higher grafting densities than in the case of two-component bottle-brushes.

The size of the cluster axial direction, *i.e.*, along the rigid backbone, has a very interesting behaviour. Looking at graphs (fig. 6a and b), we clearly see that the size of the clusters in this directions is much larger compared to that in axial direction as in the case of a single-component bottle-brush (fig. 6c). Our clusters in both cases are elongated objects as the grafting density increases. However,

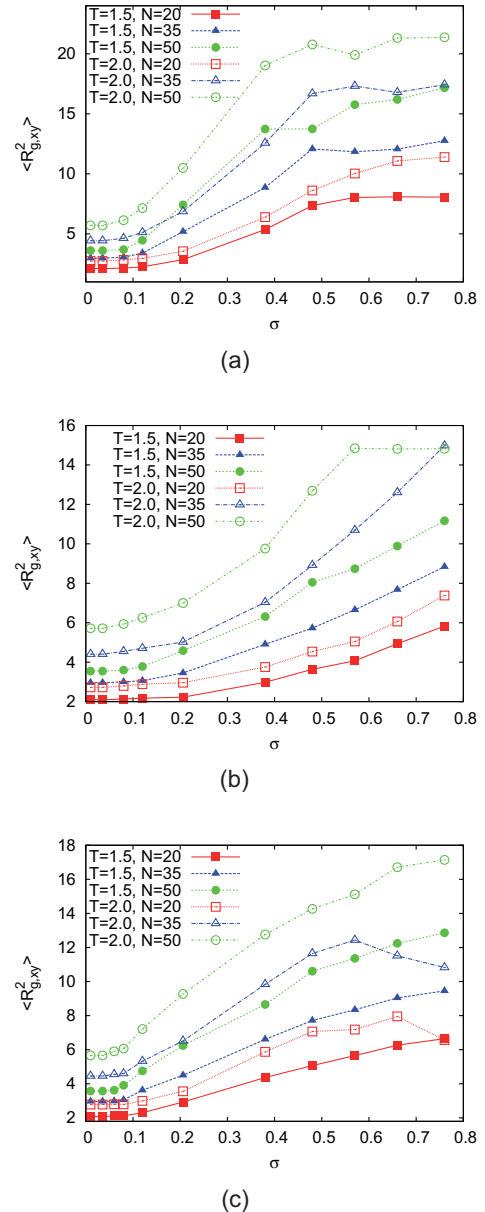


**Fig. 5.** (Colour online) The radial mean square gyration radii  $\langle R_{g,xy}^2 \rangle$  (the angular brackets denote thermal averaging) are plotted versus grafting density at  $T = 1.5$  (full symbols) and  $T = 2.0$  (open symbols) for three different chain lengths, as indicated. Case (a) refers to clusters formed from both types (A and B) of monomers, while case (b) refers to clusters formed from only one kind of monomers (A or B). (c) presents the corresponding results for the single-component bottle-brushes.

for the single-component bottle-brush the slope is higher compared to cases (a) and (b), since the side chains are of the same type and have a higher tendency to form clusters. As we have seen from fig. 2, a higher number of side chains participates in the formation of a cluster in the case of single-component bottle-brushes. The opposite effect is seen at intermediate to high grafting densities ( $\sigma > 0.4$ ) for reasons which are already described. We should note here the appearance of pronounced finite-size effects in

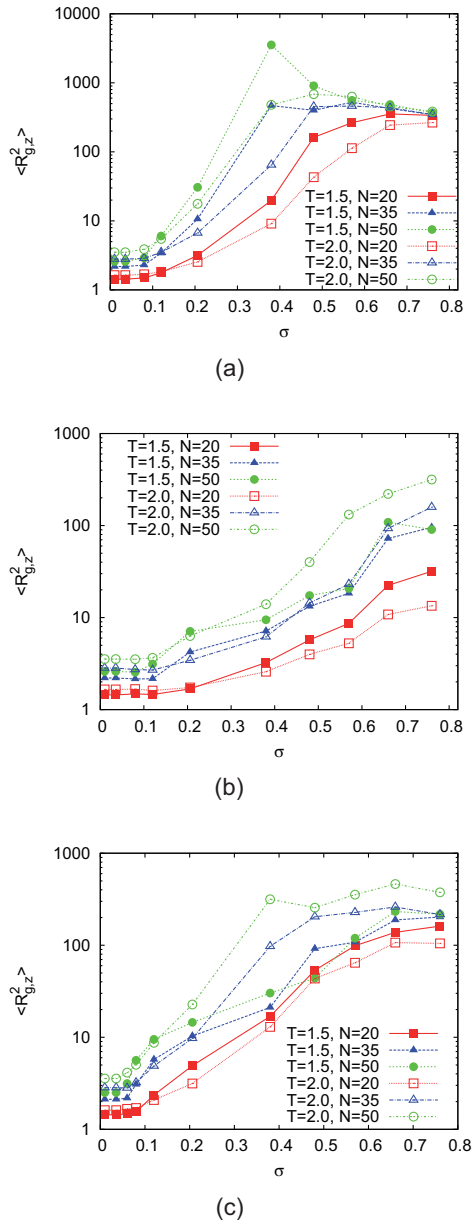


**Fig. 6.** (Colour online) Same as fig. 5, but the axial mean square gyration radii  $\langle R_{g,z}^2 \rangle$  are shown.

the case of two-component bottle-brush polymers when one defines clusters of A and B monomers already at the grafting density  $\sigma \approx 0.4$ . In fig. 6a, we can clearly see that in the region where the clusters contain a single chain the size of the clusters in the axial direction is the same as in the radial direction. The formation of pearl-necklace structure results in an extreme increase of the size of the clusters in the axial direction reaching the point where the size of the clusters is strictly dictated by the length of the backbone, that is half the length of the backbone, due to the applied periodic boundary conditions at the backbone ends. In fig. 6b it is shown clearly that the size of the clusters is small, which is expected as a smaller number of chains of the same type participate in the formation of the

cluster. Such clusters are, however, still elongated objects as a chain of type A stretches in the axial direction in order to cluster together with another A chain under poor solvent conditions. The increase of side chain length favours the increase of the size of the clusters in the axial direction, since grafted chains at higher distances are able to participate in the formation of a cluster. In fig. 6a, we observe that an increase of temperature results in the decrease of  $\langle R_{g,z}^2 \rangle$  at intermediate grafting densities (pearl-necklace regime), since the chains stretch in the radial direction. Of course, in the trivial regime, where the chains collapse individually, an increase of temperature increases the values for  $\langle R_{g,z}^2 \rangle$ . However, in fig. 6b, we observe that at intermediate to high grafting densities a different tendency with the increase of temperature occurs:  $\langle R_{g,z}^2 \rangle$  becomes higher at higher temperatures. In fact, the A chains which are far apart are able to form clusters much easier when the side chain length is high. The latter description also applies in the case of single-component bottle-brushes.

In fig. 7 the dependence of the number of clusters per side chain is presented as a function of temperature for different grafting densities and side chain lengths, always choosing the parameter combinations to be within the pearl-necklace regime. For the clusters formed from both A and B monomers (part a) in all cases the number of clusters per chain is an increasing function of temperature. This increase is stronger in the case of lower grafting densities. The same effect is seen when one considers parameter combinations in the case of clusters of A or B monomers where neither  $N$  nor  $\sigma$  are too large. However, for the combinations  $N = 35, \sigma = 0.76$ ,  $N = 50, \sigma = 0.57$  and  $N = 50, \sigma = 0.76$  a minimum in the number of clusters as a function of temperature occurs. The position of this minimum moves to larger temperatures with increasing chain length or grafting density. This effect is not restricted to the copolymer bottle-brush as a look at fig. 7c shows, where we have plotted the behaviour of homopolymer brushes at a grafting density  $\sigma = 0, 38$  corresponding to the  $\sigma = 0.76$  data from fig. 7b. For  $N = 20$  there is a monotonous increase in the number of clusters as a function of temperature, but for  $N = 35$  and  $N = 50$  we observe minima and the position again shifts to larger temperature for larger side chain length.

To understand this behaviour we have to examine in more detail how the formation of clusters induced by the collapse of the side chains below  $T = 3$  occurs. When we look at figs. 8 and 9 we observe that the clusters are formed in a rather asymmetric way. Regarding the size of the clusters in the radial direction (fig. 9), we observe that  $\langle R_{g,xy}^2 \rangle$  decreases with decrease of the temperature as expected. The variation with temperature is larger when the grafting density and the length of the side chains are higher. The same behaviour is observed in case (b) for clusters of only one type of monomer, with smaller absolute variation of course, as the clusters are smaller in the axial direction compared with the case (a), but with about the same amount of relative variation. The dependence of  $\langle R_{g,z}^2 \rangle$  on temperature is more interesting, and mirrors the

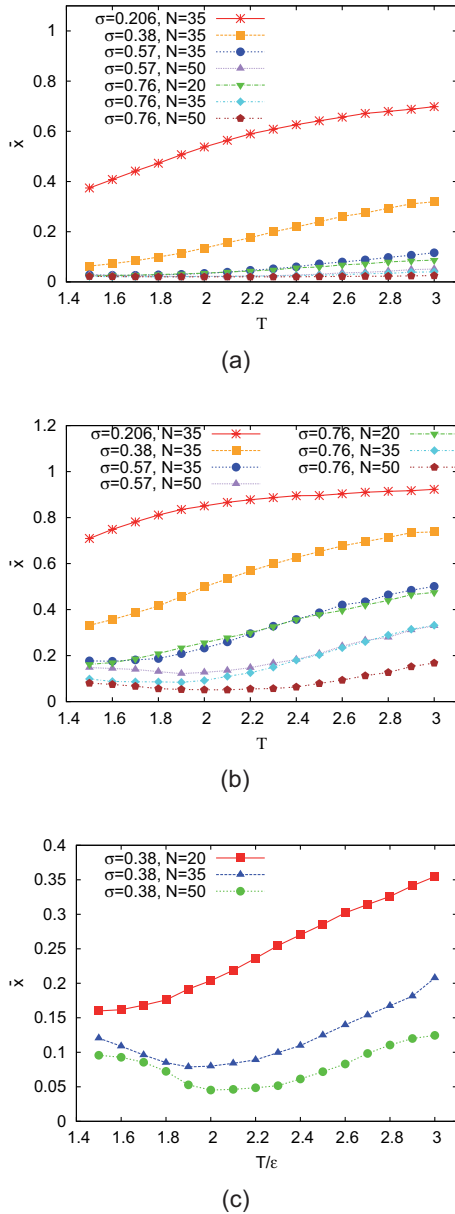


**Fig. 7.** (Colour online) The dependence of  $\bar{x}$  on temperature for various bottle-brush cases as indicated. In part (a) the case of clusters of A and B beads is shown, whereas in (b) only the case of clusters of only A or B monomers is shown. Part (c) shows results for an intermediate grafting density for the case of single-component bottle-brushes.

variation in  $\bar{x}$ . For the case of clusters made up of A and B monomers (fig. 9a) we observe relatively little variation as a function of temperature when the grafting density is rather small ( $\sigma = 0.206$ ) or large ( $\sigma \geq 0.57$ ). In the latter case the variation is larger for smaller side chain length. We observe a very strong variation (more than an order of magnitude) for the intermediate grafting density  $\sigma = 0.38$ . The axial extension of the clusters is monotonously decreasing as a function of temperature in the observed temperature window for small side chain length. For larger side chain length and higher grafting density a shallow

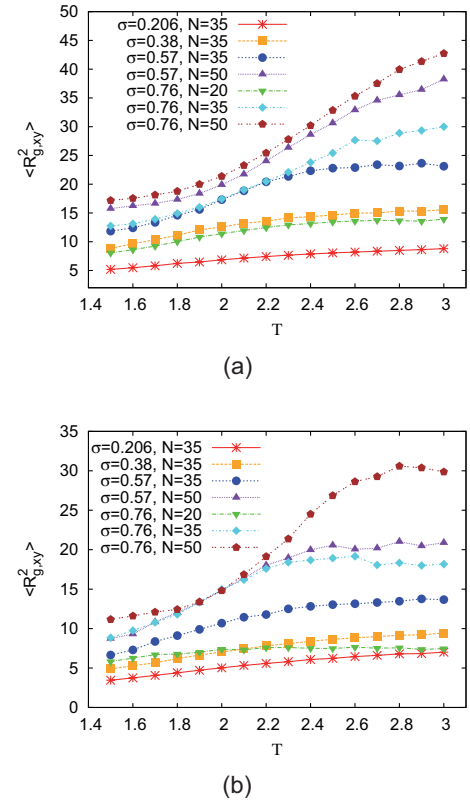


**Fig. 8.** (Colour online) Dependence of the radial mean square gyration radii on temperature for various cases as indicated in the legend.

maximum of the axial extension as a function of temperature develops. This behaviour is much more pronounced when we look at the axial size of pure A or pure B clusters in fig. 9b. In the extreme case,  $N = 50, \sigma = 0.57$ , the radial size first increases by a factor of 5, reaching a maximum around  $T = 2$ , then decreases by the same factor again.

There seem to be two physical contributions to the occurrence of this maximum in the radial extension. When the solvent quality gets poor (below  $T = 3$ ) the chains collapse but they do it in an asymmetric fashion to come into contact with neighbouring chains, which results in rather elongated clusters along the backbone of the brush (see also the snapshots in fig. 1). This elongated shape reduces the bulk free energy but has a rather large surface free energy contribution. With decreasing temperature (solvent quality) the free-energy penalty from the large surface of the elongated clusters increases and they reach a maximum size at some temperature. This explains the minima in fig. 7c and the maxima in fig. 9a. The much more pronounced maxima in fig. 9b indicate a second physical contribution. The copolymer bottle-brush exhibits local microphase separation [57] which starts to compete with the de-mixing from the solvent (collapse of the side chains). This segregation between A and B monomers breaks up the pure A or pure B clusters very effectively as the chains are grafted alternately leading to the much stronger variation in the radial extension of the pure A and B clusters observed in fig. 9b.

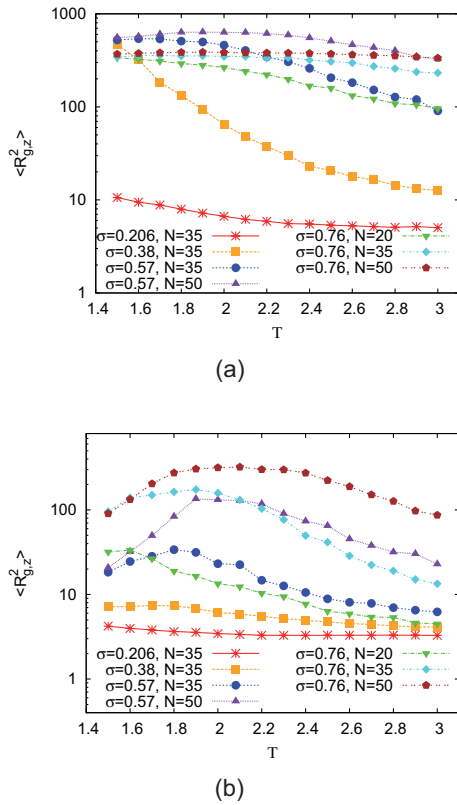


**Fig. 9.** (Colour online) Dependence of the axial mean square gyration radii on temperature for various cases as indicated in the legend.

## 4 Conclusions

In the present paper we have presented a detailed simulation study of the pearl-necklace structure that occurs for bottle-brush polymers with rigid backbones and two types of grafted side chains and moderately high grafting densities under poor solvent conditions. The combination of high local densities and large side chain lengths renders the generation of equilibrated structures in this poor solvent regime extremely difficult. We therefore chose to generate an ensemble of 500 starting structures at an elevated temperature which were then slowly cooled down to sample the properties of this system in the regime where the solvent quality becomes poor and the chains collapse onto the backbone and where simultaneously the microphase separation between A and B monomers sets in. In spite of this large simulation effort, some of our data still reveal significant statistical scatter, and it is clear from this finding that the study of even longer side chains, which might reach into the regime where scaling concepts are applicable, is out of question. We would like to stress, however, that the side chain lengths we were able to study agree nicely with the experimentally relevant range.

Since microphase separation within a “pearl” is taking place, in our analysis, we considered the clusters as a whole with A and B monomers being part of the same cluster when our neighbouring criterion between monomers is met, and we also considered clusters of only A or B beads.

Particular emphasis has been put on describing the difference between these two cases. Comparing these cases with the single-component bottle-brush, we observed that the three different cases share some similarity. The average number of clusters per chain for the clusters of A or B beads only at grafting density  $\sigma$  is the same as that of the single-component bottle-brush with grafting density  $2/\sigma$  at low temperatures.

The incompatibility between A and B monomers, however, also introduces additional effects into the geometry of the clusters as a function of temperature and grafting density. Whereas the axial extension of A and B clusters and of homopolymer clusters is rather similar, the radial extension behaves differently. For the homopolymer brush, the radial size is a monotonously increasing function of grafting density, whereas for the copolymer brush, the A and B clusters display a maximum radial extension around  $\sigma = 0.5$  for long enough side chains and low temperatures, induced by the tendency for microphase separation for large densities and side chain lengths. Similarly, the maximum in the radial extension of the pure A or pure B clusters as a function of temperature is much more pronounced than for the homopolymer case or the A and B clusters, since here microphase separation tendency and reduction in surface free energy both contribute to this effect.

Our results give some first overview of the intricate interplay between de-mixing from a poor solvent and microphase separation occurring in copolymer bottle-brushes and on the effects of these phase changes on the pearl-necklace structure of a bottle-brush polymer at intermediate grafting densities. It is also interesting to compare the microphase separations occurring in our quasi-one-dimensional system, where due to the low dimensionality sharp phase transitions in a strict thermodynamic sense are impossible, as discussed in more detail elsewhere [47], to the corresponding system of polymers grafted to flat planar substrates under poor solvent conditions at intermediate grafting densities. Simulations have revealed a corresponding microphase separation where several chains aggregate together into clusters also in this case [77,78] and phenomenological mean-field-type theories have predicted the resulting phase diagram [79–81]. For binary (A, B) brushes self-consistent field theories predict a variety of long-range ordered structures, similar to the mesophases of block copolymers [82]. However, it was noted [83] that the randomness in the local density of grafting sites precludes the occurrence of true long-range order. Thus, we expect that qualitatively the behavior of mixed planar brushes in poor solvents and comparable chain lengths and grafting densities would actually be rather similar to the present system.

One of us (P.E.T.) gratefully acknowledges financial support through a Max-Planck-fellowship awarded by the Max Planck Institute for Polymer Research. The computer simulations were carried out on the Juropa supercomputer under the HMZ03 project and the SoftComp NoE computer cluster at the Jülich Supercomputing Centre. We thank the John von Neumann Institute for Computing for the allocation of computing time.

## References

1. M. Zhang, A.H.E. Müller, *Polym. Sci. Part. A: Polym. Chem.* **43**, 3461 (2005).
2. S.S. Sheiko, B.S. Sumerlin, K. Matyjaszewski, *Progr. Polym. Sci.* **33**, 759 (2008).
3. M. Wintermantel, M. Schmidt, Y. Tsukahara, K. Kajiwara, S. Kahijiya, *Makromol. Chem., Rapid Commun.* **15**, 279 (1994).
4. M. Wintermantel, M. Gerle, K. Fischer, M. Schmidt, I. Wataoka, H. Urakawa, K. Kajiwara, Y. Tsukahara, *Macromolecules* **29**, 978 (1996).
5. K.L. Beers, S.G. Gaynor, K. Matyjaszewski, S.S. Sheiko, M. Möller, *Macromolecules* **31**, 9431 (1998).
6. S. Lecommandoux, F. Chilecot, R. Borsali, M. Schapacher, A. Deffieux, A. Brulet, J.P. Cotton, *Macromolecules* **35**, 8878 (2002).
7. T. Stephan, S. Muth, M. Schmidt, *Macromolecules* **35**, 9875 (2002).
8. Y. Liu, V. Aleetz, A.H.E. Müller, *Macromolecules* **36**, 7894 (2003).
9. C. Li, N. Gunari, K. Fischer, A. Janshoff, M. Schmidt, *Angew. Chem. Int. Ed.* **43**, 1101 (2004).
10. S. Rathgeber, T. Pakula, K. Matyjaszewski, K.L. Beers, *J. Chem. Phys.* **122**, 129404 (2005).
11. B. Zhang, F. Gröhn, J.S. Pedersen, K. Fischer, M. Schmidt, *Macromolecules* **39**, 8440 (2006).
12. L. Feuz, P. Strunz, T. Gene, M. Textor, O. Borisov, *Eur. Phys. J. E* **23**, 237 (2007).
13. H.I. Lee, K. Matyjaszewski, S. Yu-Su, S.S. Sheiko, *Macromolecules* **41**, 6073 (2008).
14. R.V. Iozzo (Editor), *Proteoglycans: Structure, Biology and Molecular Interactions* (Marcel Dekker, New York, 2000).
15. H. Muir, *Biochem. Soc. Trans.* **11**, 613 (1983).
16. N.C. Kaneider, S. Dunzendorfer, C.J. Wiedermann, *Biochemistry* **43**, 237 (2004).
17. J. Klein, *Science* **323**, 47 (2009).
18. T.M. Birshstein, E.B. Zhulina, *Polymer* **25**, 1453 (1984).
19. T. Witten, P.A. Pincus, *Macromolecules* **19**, 2509 (1986).
20. T.M. Birshstein, O.V. Borisov, E.B. Zhulina, A.R. Khokhlov, T.A. Yurasowa, *Polym. Sci. USSR* **29**, 1293 (1987).
21. Z.G. Wang, S.A. Safran, *J. Chem. Phys.* **89**, 5323 (1988).
22. C. Ligoure, L. Leibler, *Macromolecules* **23**, 5044 (1990).
23. R.C. Ball, J.F. Marko, S.T. Milner, T.A. Witten, *Macromolecules* **24**, 693 (1991).
24. M. Murat, G.S. Grest, *Macromolecules* **24**, 704 (1991).
25. N. Dan, M. Tirrell, *Macromolecules* **25**, 2980 (1992).
26. C.M. Wijmans, E.B. Zhulina, *Macromolecules* **26**, 7214 (1993).
27. G.H. Fredrickson, *Macromolecules* **26**, 2825 (1993).
28. H. Li, T.A. Witten, *Macromolecules* **27**, 449 (1994).
29. E.B. Zhulina, T.A. Vilgis, *Macromolecules* **29**, 2605 (1996).
30. Y. Rouault, O.V. Borisov, *Macromolecules* **29**, 2605 (1996).
31. E.M. Sevick, *Macromolecules* **29**, 6952 (1996).
32. M. Saariaho, O. Ikkala, I. Szleifer, I. Erukhimovich, G. ten Brinke, *J. Chem. Phys.* **107**, 3267 (1997).
33. M. Saariaho, I. Szleifer, O. Ikkala, G. ten Brinke, *Macromol. Theory Simul.* **7**, 211 (1998).
34. Y. Rouault, *Macromol. Theory Simul.* **7**, 359 (1998).
35. M. Saariaho, A. Subbotin, I. Szleifer, O. Ikkala, G. ten Brinke, *Macromolecules* **32**, 4439 (1999).
36. K. Shiokawa, K. Itoh, N. Nemoto, *J. Chem. Phys.* **111**, 8165 (1999).
37. A. Subbotin, M. Saariaho, O. Ikkala, G. ten Brinke, *Macromolecules* **33**, 3447, (2000).
38. P.G. Khalatur, D.G. Shirvanyanz, N.Y. Staroviotovo, A.R. Khokhlov, *Macromol. Theory Simul.* **9**, 141 (2000).
39. R. Stepanyan, A. Subbotin, G. ten Brinke, *Macromolecules* **35**, 5640 (2002).
40. N.A. Denesyuk, *Phys. Rev. E* **67**, 051803 (2003).
41. J. de Jong, G. ten Brinke, *Macromol. Theory Simul.* **13**, 318 (2004).
42. S. Elli, F. Ganazzoli, E.G. Timoshenko, Y.A. Kuznetsov, R. Connolly, *J. Chem. Phys.* **120**, 6257 (2004).
43. S.S. Sheiko, O.V. Borisov, S.A. Prokhorova, M. Möller, *Eur. Phys. J. E* **13**, 125 (2004).
44. R. Connolly, G. Bellesia, E.G. Timoshenko, Y.A. Kuznetsov, S. Elli, F. Ganazzoli, *Macromolecules* **38**, 5288 (2005).
45. A. Yethiraj, *J. Chem. Phys.* **125**, 204901 (2006).
46. H.-P. Hsu, W. Paul, K. Binder, *Europhys. Lett.* **76**, 526 (2006).
47. H.-P. Hsu, W. Paul, K. Binder, *Macromol. Theory Simul.* **16**, 660 (2007).
48. A.V. Subbotin, A.N. Semenov, *Polym. Sci., Ser. A* **49**, 1326 (2007).
49. H.-P. Hsu, W. Paul, K. Binder, *J. Chem. Phys.* **129**, 204904 (2007).
50. I.I. Potemkin, V.V. Palyulin, *Polym. Sci. Ser. A* **51**, 163 (2009).
51. P.E. Theodorakis, W. Paul, K. Binder, *EPL* **88**, 63002 (2009).
52. H.-P. Hsu, K. Binder, W. Paul, *Phys. Rev. Lett.* **103**, 198301 (2009).
53. H.-P. Hsu, W. Paul, S. Rathgeber, K. Binder, *Macromolecules* **43**, 1592 (2010).
54. H.-P. Hsu, W. Paul, K. Binder, *Macromolecules* **43**, 3094 (2010).
55. P.E. Theodorakis, W. Paul, K. Binder, *Macromolecules* **43**, 5137 (2010).
56. P.E. Theodorakis, W. Paul, K. Binder, *J. Chem. Phys.* **133**, 104901 (2010).
57. I. Erukhimovich, P.E. Theodorakis, W. Paul, K. Binder, *J. Chem. Phys.* **134**, 054906 (2011).
58. V.V. Vasilevskaya, A.A. Klochov, P.G. Khalatur, A.R. Khokhlov, G. ten Brinke, *Macromol. Theory Simul.* **10**, 389 (2001).
59. P.A. Janmey, J.F. Leterrier, H. Hermann, *Curr. Opin. Colloid Interface Sci.* **8**, 40 (2003).
60. R. Chang, Y. Kwak, Y. Gebremichael, *J. Mol. Biol.* **391**, 648 (2009).
61. W. Stevenson, R. Chang, Y. Gebremichael, *J. Mol. Biol.* **405**, 1101 (2011).
62. E.B. Zhulina, F.A.M. Leermakers, *Biophys. J.* **93**, 1421 (2007).
63. D.H. Napper, *Polymeric Stabilization of Colloidal Dispersions* (Academic, London, 1983).
64. K. Ohno, T. Morinaga, S. Takeno, Y. Tsujii, T. Fukuda, *Macromolecules* **40**, 9143 (2007).
65. A. Polotsky, M. Charlaganov, Y.Y. Xu, F.A.M. Leermakers, M. Daoud, A.H.E. Müller, T. Dotera, O. Borisov, *Macromolecules* **41**, 4020 (2008).

66. G.S. Grest, K. Kremer, *Phys. Rev. A* **33**, 3628 (1986).
67. G.S. Grest, M. Murat, in *Monte Carlo and Molecular Dynamics Simulations in Polymer Science*, edited by K. Binder (Oxford University Press, New York, 1995) p. 476.
68. G.S. Grest, *Adv. Polym. Sci.* **138**, 149 (1999).
69. M. Murat, G.S. Grest, *Macromolecules* **22**, 4054 (1989).
70. G.S. Grest, M. Murat, *Macromolecules* **26**, 3108 (1993).
71. G.S. Grest, *Macromolecules* **27**, 418 (1994).
72. S.K. Das, J. Horbach, K. Binder, *J. Chem. Phys.* **119**, 1547 (2003).
73. <http://www.gromacs.org>.
74. W.F. van Gunsteren, H.J.C. Berendsen, *Mol. Simul.* **1**, 173 (1988).
75. L.D. Landau, E.M. Lifshitz, *Statistical Physics* (Pergamon Press, Oxford, 1959).
76. F.H. Stillinger, *J. Chem. Phys.* **38**, 1486 (1963).
77. P.-Y. Lai, K. Binder, *J. Chem. Phys.* **97**, 586 (1992).
78. G.S. Grest, M. Murat, *Macromolecules* **26**, 3108 (1993).
79. C. Yeung, A.C. Balazs, D. Jasnow, *Macromolecules* **26**, 1914 (1993).
80. H. Tang, I. Szleifer, *Europhys. Lett.* **28**, 19 (1994).
81. M.A. Carignano, I. Szleifer, *J. Chem. Phys.* **100**, 3210 (1994).
82. M. Müller, *Phys. Rev. E* **65**, 030802(R) (2002).
83. L. Wenning, M. Müller, K. Binder, *Europhys. Lett.* **71**, 639 (2005).